Cellular Internalization of Quantum Dots Mediated by Cell-Penetrating Peptides

Betty Revon Liu[1], Huey-Jenn Chiang[2], Yue-Wern Huang[3], Ming-Huan Chan[4], Hwei-Hsien Chen[5] and Han-Jung Lee[1,*]

[1]*Department of Natural Resources and Environmental Studies,* [2]*Institute of Biotechnology, National Dong Hwa University, Hualien 97401, Taiwan;* [3]*Department of Biological Sciences, Missouri University of Science and Technology, Rolla, MO 65409-1120, USA;* [4]*Institute of Neuroscience, National Chengchi University, Taipei 11605, Taiwan;* [5]*Institute of Population Health Sciences, National Health Research Institutes, Miaoli 35053, Taiwan*

Abstract: Nanomaterials have been utilized in biomedical applications for many years because of their unique properties such as quantum confinement, surface plasmon resonance, and superparamagnetism. These applications are expected to advance diagnosis and therapeutics. Fluorescent nanomaterials, such as quantum dots (QDs), were exalted in biological imaging and tracking, and trended to replace protein-based probes. Our previous investigation indicated that cell-penetrating peptides (CPPs) are a promising delivery system that can translocate materials efficiently in a noncovalent manner. In this study, we demonstrate that arginine-rich CPPs can noncovalently complex with QDs and significantly raise efficiency of cellular entry. We further examined their mechanisms of cellular penetrations, subcellular localizations, and cytotoxicity. Importantly, CPP/QD complexes were not toxic at the level of efficient transduction. Collectively, our study provided an insight that CPPs can facilitate the delivery of nanomaterials into cells. Various compositions of CPPs are a major factor affecting uptake routes and efficiency for drug delivery applications.

Keywords: Cell-penetrating peptides, pharmacological inhibitors, polyarginine, protein transduction, quantum dots.

INTRODUCTION

Nanomaterials are defined as materials with at least one dimension in the range of 1-100 nm. By definition, they include artificial materials (such as inorganic element-based nanoplatforms and liposomes) and natural materials (such as proteins and DNAs). In recent years, advancements in synthesis and surface modification of inorganic element-based nanomaterials have provided a wide spectrum of products for various industries, such as cosmetics, painting, constructions, electronics, and biomedicine. According to their physicochemical properties, inorganic element-based nanomaterials used in biomedical applications include metals, semiconductors, or bionic matters [1, 2]. They can be used for diagnosis and therapeutics. The applications of inorganic element-based nanomaterials in medicine take advantage of their tunable optical, electronic, magnetic, and biologic properties [1]. For instance, oligonucleotide-modified or antibody-modified nanoparticles, and optical nanostructures can serve as probes in basic research and diagnosis. Optical and fluorescent nanomaterials have been extensively applied for imaging purposes [1, 3, 4].

As traditional organic dyes and fluorescent proteins are limited to short-term imaging applications, inorganic semiconductor nanoparticles (also known as quantum dots; QDs) are ideal for long-term tracking and imaging purpose. Advantages of QDs include, but are not limited to, wide spectral range of excitation, composition-tunable emission, high levels of brightness, resistance to photobleaching and chemical degradation, and ultrasensitive detection [5-7]. Using two-photon excitation microscopy, QDs can yield high quality of deep tissue imaging [8]. One of the drawbacks is that QDs enter living cells in a very slow pace. Many techniques, such as microinjection, electroporation, and liposome-based transduction, have been used to improve QD transduction efficiency [9, 10]. Further, QDs tend to aggregate and are trapped in endosomes or vesicles after cellular internalization [7, 11, 12]. Thus, improvement of QD solubility and uptake efficiency for biomedical applications must be sought. Peptide conjugation has evolved as an efficient tool to solve such problems [13, 14].

Cell-penetrating peptides (CPPs), also called protein transduction domains (PTDs) or arginine-rich intracellular delivery (AID) peptides, are capable of overcoming impermeable plasma membranes to deliver biologically active molecules [15-19]. The specific domain of this protein transduction function was first identified from the human immunodeficiency virus type 1 (HIV-1) transcriptional activator Tat protein [15, 16]. Development of various CPPs derived from Tat protein has sprung up in recent decades [17-19]. These CPPs can be cationic, amphipathic, or hydrophobic peptides [20]. Our previous studies indicated that CPPs had the potential to deliver biomolecules as cargoes into cells in a covalent, noncovalent, or covalent and noncovalent protein transductions (CNPT) manners [21-24]. CPP-functionalized QDs can be prepared by either covalent conjugation or noncovalent interactions [25]. Covalent cou-

*Address correspondence to this author at the Department of Natural Resources and Environmental Studies, National Dong Hwa University, No. 1, Sec. 2, Da-Hsueh Road, Shoufeng Township, Hualien 97401, Taiwan; Tel: +886 3 8633642; Fax: +886 3 8633260; E-mail: hjlee@mail.ndhu.edu.tw

2211-7393/13 $58.00+.00

pling methods tend to produce larger nanoparticles (10-50 nm) with greater colloidal stability [26], increase the solubility of QDs, and consequently the efficiency of transduction delivery [27]. In contrast, noncovalent approaches are simple and produce smaller nanoparticles (< 10 nm); however, the weak binding between peptides and QDs may result in poor colloidal stability [28]. CPPs can deliver cargoes with sizes up to 200 nm in diameter [29]. Cargoes include proteins, DNAs, RNAs, peptide nucleic acids (PNAs), small molecular drugs, inorganic particles, and liposomes [13, 29-46]. The target objects, which CPPs and their cargoes were able to penetrate, were in a wide range of different species from prokaryocytes to eukaryocytes [21-24, 32-46]. Rapid cellular entry of CPPs was measured at a half-time of 1.8 min, corresponding to a first-order rate constant of 0.007 sec^{-1}, and their concentrations for bioapplication could be up to 100 μM without causing injury to cells [47, 48]. Based upon their high transduction efficiency, fast transduction rate, and low cytotoxicity, CPPs have been tested in clinical trials [19].

To date, there are two major routes of CPP penetration: direct membrane translocation and endocytosis-mediated pathway [49]. Energy-dependent endocytosis includes classical clathrin-, caveolae-dependent endocytosis, and nonclassical macropinocytosis. Pharmacological and other biologically active molecules delivered via this process may be trapped and degraded in lysosomes [50, 51]. As QDs have potential for biological research, it is essential to understand the QD-mediated internalization process that depends on their conjugated peptides or molecules [52]. The endocytic process usually involves vesicular trapping in cells, and escape from endosomal/lysosomal vesicles becomes important for CPP-delivered cargoes in biomedical applications [53]. Thus, CPP-mediated endosomal disruption by agents, such as chloroquine, was used to promote endosomal escape [53-55].

In this report, we studied cellular internalization of QDs mediated by four CPPs with different amino acid compositions. Noncovalent interactions between QDs and CPPs resulted in net positive charges which favor cellular entry of CPP/QD complexes. We further investigated mechanisms of cellular internalization, subcellular localization, and cytotoxicity of these four CPP/QD complexes.

METHODS AND MATERIALS

Preparation of QDs and Peptides

Carboxyl-functionalized CdSe/ZnS QDs with the maximal emission peak at 525 nm wavelength (eFluor 525NC) were purchased from eBioscience (San Diego, CA, USA) [25, 38, 39]. Four arginine-rich CPPs, SR9 (R9), HR9 (CH5-R9-H5C), PR9 (FFLIPKG-R9), and IR9 (GLFEAIEGFIENGWEGMIDGWYG-R9), vary in sequence compositions but with a R9 consensus segment (Genomics, Taipei, Taiwan) [40, 42-46].

Gel Retardation Assay

To determine noncovalent interactions between CPPs and QDs, various amounts (from 0 to 600 μM) of PR9 and IR9 were mixed with 2 μM of QDs in phosphate buffered saline (PBS) and then incubated at 37℃ for 2 h. Various molecular ratios of CPP/QD complexes from 0 to 300 were analyzed by electrophoresis on a 0.5% agarose gel (Multi ABgarsoe, ABgene, UK) in 0.5 × TAE buffer (40 mM of Tris-acetate and 1 mM of EDTA, pH 8.0) at 100 V for 40 min [38]. Images were captured using a Typhoon FLA 9000 biomolecular imager (GE Healthcare, Piscataway, NJ, USA) with the excitation wavelength at 473 nm of a LD laser and with the emission wavelength above 473 nm by a LPB filter. All data were analyzed using ImageQuant TL 7.0 software (GE Healthcare).

Particle Size and Zeta-Potential Measurement

CPPs (12.4 μM of SR9, HR9, PR9, or IR9) and 100 nM of QDs were separately dissolved in double deionized water. Then, QDs were mixed with SR9, HR9, or PR9 at a molecular ratio of 60, or with IR9 at molecular ratios of 60, 120, and 240. Each solution was equilibrated at 25℃ for 120 sec. The sizes and zeta-potentials of QDs alone and CPP/QD complexes were analyzed using a Zetasizer Nano ZS equipped with Zetasizer software 6.30 (Malvern Instruments Ltd., Malvern, Worcestershire, UK).

Cell Culture

Human bronchoalveolar carcinoma A549 cells (American Type Culture Collection, Manassas, VA, USA; CCL-185) were cultured in Roswell Park Memorial Institute (RPMI) 1640 medium (Gibco, Invitrogen, Carlsbad, CA, USA) supplemented with 10% (v/v) bovine serum (Gibco) in a humidified incubator with 5% CO_2 at 37℃ [22].

Chemicals

5-(*N*-ethyl-*N*-isopropyl)-amiloride (EIPA), cytochalasin D (CytD), filipin, nocodazole, valinomycin, *N*-ethylmaleimide (NEM), sodium chlorate ($NaClO_3$), methyl-β-cyclodetritrin (MβCD), nystatin, and chloroquine were purchased from Sigma-Aldrich (St. Louis, MO, USA), while nigericin and sodium azide were from Fluka Chemie (Seelze, Germany). Hoechst 33342, LysoTracker DND-99, and Texas Red-X Phalloidin were purchased from Invitrogen, while rabbit anti-human early endosome antigen 1 protein (EEA1) antibody and goat Alexa Fluor 647-conjugated anti-rabbit antibody fragment were from Cell Signaling (Danvers, MA, USA).

Delivery of CPP/QD Complexes into Cells

To test the protein transduction of CPP/QD complexes, three CPPs (SR9, HR9, and PR9) were mixed with QDs at a molecular ratio of 60 for 2 h. IR9 was mixed with QDs at molecular ratios of 60 and 120. After complex formation, all mixtures were incubated with A549 cells for 1 and 24 h at 37℃. In kinetics of transduction, 100 nM of QDs alone or 100 nM of QDs were incubated with 6 μM of SR9, HR9, PR9, or IR9, followed by incubation with A549 cells for a period of 30 min, 1, 2, 3, 4, 5, and 24 h at 37℃.

To inhibit endocytosis, physical and pharmacological endocytic modulators were used [38-40]. For physical inhibition, all reagents were prepared at 4℃, and cells were placed at 4℃ for 30 min to deplete energy required by all

endocytic pathways. CPP/QD complexes were added to cells and then incubated at 4℃ for 30 min. For pharmacological inhibition, cells were pretreated with 100 μM of EIPA to disrupt macropinocytosis, 10 μM of CytD to block F-actin rearrangements, 5 μg/mL of filipin to inhibit caveolae-dependent endocytosis, or 10 μM of nocodazole to impair microtubule polymerization for 30 min. Then, cells were treated with CPP/QD complexes for 30 min.

For further investigation of cellular uptake of SR9/QD complexes, more endocytic modulators were examined by treating cells with effective concentrations for 1 h at 37℃ prior to treating with SR9/QD complexes as described above. Cells were treated with 2 μM of nigericin or valinomycin to dissipate membrane potential, 10 mM of sodium azide to inhibit energy-dependent molecular movement, 1 mM of NEM to disrupt clatharin- and caveolae-dependent pathways, or 80 mM of $NaClO_3$ to inhibit energy-dependent pathway [38]. For lipid and cholesterol sequestration, cells were treated with 2 mM of MβCD or 5 μg/mL of nystatin.

To study lysosomal escape and cellular uptake enhancement, a lysosomotropic agent chloroquine was utilized [40]. Cells were treated with either 100 nM of QDs alone or 6 μM of CPPs (SR9, HR9, or PR9) mixed with QDs in the absence or presence of 25 or 100 μM of chloroquine at 37℃ for 2 h. Cellular uptake was then measured by flow cytometry.

Subcellular Colocalization

For subcellular colocalization studies, Hoechst 33342, LysoTracker DND-99, Texas Red-X Phalloidin, rabbit anti-human EEA1 antibody and goat Alexa Fluor 647-conjugated anti-rabbit antibody fragment were used to visualize nucleus, lysosome, F-actin, and early endosome, respectively [38, 40]. EEA1 rabbit antibody and goat Alexa Fluor 647-conjugated anti-rabbit antibody fragment were the first and second antibodies to visualize the location of early endosomes. Cells were treated with CPP/QD complexes for time courses of 30 min, 1, 2, 3, 4, and 5 h at 37℃, followed by 3.7% formaldehyde fixation. Cells were stained with specific fluorescent probes according to the manufacturers' instructions.

Fluorescent and Confocal Microscopy

Fluorescent and bright-field images were observed and recorded using an Olympus IX70 inverted fluorescent microscope (Olympus, Center Valley, PA) [38] or a BD Pathway 435 System (BD Biosciences, Franklin Lakes, NJ, USA) [40]. Excitation filters were set at 377/50 nm, 482/35 nm and 543/22 nm for blue, green and red fluorescence, respectively. Emission filters were set at 435LP (long-pass), 536/40 nm and 593/40 nm for blue (BFP), green (GFP) and red fluorescent protein (RFP) channels, respectively. Bright-field microscopy was used to assess cell morphology.

Flow Cytometric Analysis

Human A549 cells were seeded at a density of 2.5×10^5 per well in 24-well plates. Control and the experimental groups were then harvested and analyzed using a Cytomics FC500 flow cytometer (Beckman Coulter, Fullerton, CA) with FL1 filters (excitation at 488 nm and emission at 513 nm) [33]. Data were analyzed using CXP software. Results are reported as the percentage of total cell population.

Cytotoxicity Measurement

Cells were treated with QDs or CPP/QD complexes for 24 h at 37℃. At the end of the experiment, cell medium was removed, and cells were then washed several times with PBS. Cell viability was determined using the sulforhodamine B (SRB) assay [23].

Statistical Analysis

Data are presented as mean ± standard deviations (SDs). Statistical comparisons between the control and experimental groups were performed using the Student's *t*-test. Mean values and SDs were calculated from data of at least three independent experiments. The level of statistical significance is set at $P < 0.05$ (*, †) or 0.01 (**, ††).

RESULTS

In vitro Interactions between CPPs and QDs

Gel retardation assays were conducted to determine whether CPPs can form stable complexes with QDs. PR9 and IR9 peptides were mixed and incubated with carboxylated QDs in different CPP/QD ratios (0, 15, 30, 60, 90, and 120). Results showed that PR9 and IR9 interacted with QDs noncovalently, and the shifts of CPP/QD complexes depended on the amount of CPPs added (Fig. **1**). Complexes could be completely retarded with the increasing amounts of CPPs at molecular ratios of 60 or above during electrophoresis. These data indicate that the optimal combination ratio of CPP/QD complexes is 60; accordingly, and this ratio is used in subsequent experiments.

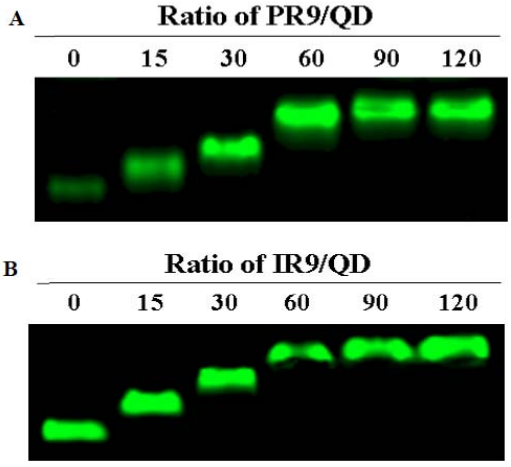

Fig. (1). Gel retardation of CPP/QD complexes (**A**). Gel retardation of PR9/QD complexes prepared at different combination ratios of 0 (QDs alone), 15, 30, 60, 90, and 120. (**B**). Gel retardation of IR9/QD complexes at different combination ratios (0, 15, 30, 60, 90, and 120). After incubation at 37℃ for 2 h, all mixtures were analyzed by electrophoresis on a 0.5% agarose gel. Fluorescence of QDs was visualized at 473 nm with Typhoon FLA 9000 biomolecular imager.

Characteristics of CPP/QD Complexes

To analyze the sizes of complexed particles, QDs alone or CPP/QD complexes prepared at a molecular ratio of 60 were measured using a Zetasizer. The core of QDs was 2.0 ± 0.1 nm in diameter (Fig. **2A**). Addition of CPPs increased its size: SR9/QD, HR9/QD, and PR9/QD complexes exhibited similar sizes of 15.7 ± 1.1 nm (Fig. **2B**-**D**), while IR9/QD complexes showed an average size of 13.5 ± 0.9 nm in diameter (Fig. **2E**). To determine surface charge of different CPP/QD complexes, QDs alone, CPPs alone, CPP/QD complexes prepared at a molecular ratio of 60 (SR9/QD, HR9/QD, and PR9/QD), or IR9/QD complexes formed at molecular ratios of 60, 120, and 240 were measured using a Zetasizer. Carboxyl-functionalized QDs exhibited negative charge, while arginine-rich CPPs (SR9, HR9, PR9, and IR9) displayed positive charges (Fig. **3A**). HR9/QD and PR9/QD complexes (28.0 ± 3.2 and 21.7 ± 1.1 mV) yielded more positive charges than those of SR9/QD and IR9/QD complexes (8.4 ± 0.2 and 3.7 ± 1.2 mV) (Fig. **3A**). As molecular ratio of IR9/QD complexes increased to 120 and 240, zeta-potentials increased (14.3 ± 0.5 and 16.6 ± 1.5 mV) (Fig. **3B**). These data demonstrate that CPP/QD complexes have the potential to cross the negative-charged cytoplasmic membrane and be translocated into A549 cells.

Delivery of CPP/QD Complexes into Cells

To confirm the protein transduction ability of CPPs in QDs delivery, we analyzed the kinetics of cellular internalization of CPP/QD complexes. At 1 h, the HR9 group showed 1.6 and 5 times higher than those of SR9 and PR9 uptake, respectively (Fig. **4**). At 24 h, the protein transduction efficiency of SR9, HR9, and PR9 in delivering QDs was similar (Fig. **4**). The significantly lower IR9-mediated QD delivery might result from comparatively lower zeta-potential of the complexes (Fig. **3B** and **4**).

Mechanisms of Cellular Uptake of CPP/QD Complexes

To identify the delivery mechanisms of CPP/QD complexes, we used physical and pharmacological modulators. None of these modulators reduced the entry of HR9/QD complexes, indicating the mechanism of direct membrane translocation (Fig. **5A**). Most modulators (except EIPA) reduced the population of positive cells in PR9/QD complexes, indicating an energy-dependent endocytic pathway. The penetration of SR9/QD complexes was reduced by low temperature and EIPA.

To further investigate the cellular delivery of SR9/QD complexes, additional endocytic modulators were utilized. For energy-dependent process, cells treated with different process modulators, such as nigericin, valinomycin, low temperature, sodium azide, sodium chlorate, nocodazole, and NEM, showed 135.2 ± 29.5%, 97.5 ± 34.4%, 90.4 ± 19.4%, 75.3 ± 30.4%, 74.1 ± 51.4%, 155.2 ± 45.9%, and 117.4 ± 59.9% of population with positive cells, respectively (Fig. **5B**). These modulators did not present significant differences comparing to the control. Clathrin- and caveolae-related modulators, such as nocodazole, NEM, MβCD, CytD, filipin, and nystatin were used, but no significant difference was found between the control and the groups treated with NEM, filipin, and CytD (117.4 ± 59.9%, 93.8 ± 56.1%, and 146.9 ± 38.8%, respectively). Moreover, the microtubule depolymerization agonist nocodazole did not show significant effect. Lipid-raft related modulators, such as filipin, nystatin, and MβCD, showed no significant differences in SR9/QD complex delivery. Nystatin and EIPA reduced the fluorescent population (42.0 ± 16.9%, and 39.6 ± 26.4%, respectively), but MβCD enhanced the cellular uptake of SR9/QD complexes (157.1 ± 26.8%). Collectively, cellular internalization of SR9/QD complexes seemed to go by a combination of multiple internalization pathways, while macropinocytosis is a major route.

Chloroquine, a lysosomotropic agent, was used to investigate lysosomal escape of CPP/QD complexes. Cells were treated with either QDs alone or CPP/QD complexes in the absence or presence of chloroquine for 2 h, followed by detection of flow cytometry. No enhancement in uptake of HR9/QD complexes was found, supporting findings of direct membrane translocation for HR9/QD complexes (Fig. **6**). Chloroquine facilitated lysosomal escape of PR9/QD complexes (Fig. **6**). Significant increase in uptake of SR9/QD complexes was only observed in the cells treated with 25 μM of chloroquine. Ascending population of fluorescent cells in chloroquine-treated groups of QDs alone, SR9/QD, and PR9/QD complexes provided additional evidence that the transduction of QD, SR9/QD, and PR9/QD complexes was an endocytosis-based process.

Time-Dependent Intracellular Distributions of CPP/QD Complexes

To determine subcellular localizations of CPP-delivered QDs and their trafficking, cells were treated with either QDs alone or with CPP/QD complexes, and stained with organelle-specific fluorescent markers, such as Hoechst 33342, Texas Red-X Phalloidin, LysoTracker DND-99, and immunofluorescent EEA1 antibody to visualize nuclei, F-actins, lysosomes, and early endosomes, respectively. In F-actin colocalization, the merged images showed that QDs alone, SR9/QD, and HR9/OD complexes were associated with neither nuclei nor F-actins in early periods of time (Fig. **7A**-**C**). Although some yellow spots were seen in the merged images of HR9/QD groups at 3-5 h treatments (Fig. **7C**), there was no colocalization between HR9/QD complexes and F-actin in confocal images (data not shown). Some orangey filaments in the cells treated with PR9/QD complexes were found, and PR9/QD complexes were highly associated with F-actin from 30 min to 5 h after transduction delivery (Fig. **7D**). These results indicate that internalization of PR9/QD complexes involves actin-related endocytosis.

Further studies involved subcellular localizations of CPP/QD complexes and their associations with lysosomes. No yellow or orange spots were observed in the merged images of QDs alone or HR9/QD complexes from 30 min to 5 h, indicating neither QD alone nor HR9/QD complexes were trapped in lysosomes (Fig. **8A** and **C**). However, punctate cells with yellow/orange color were seen after a 3 h treatment of SR9/QD complexes, meaning those SR9/QD complexes did not stay in lysosomes in early stage of protein transduction but trapped by lysosomes in the late stage (Fig. **8B**). In groups of PR9-mediated QDs delivery, yellow/orange spots were observed in the merged images from

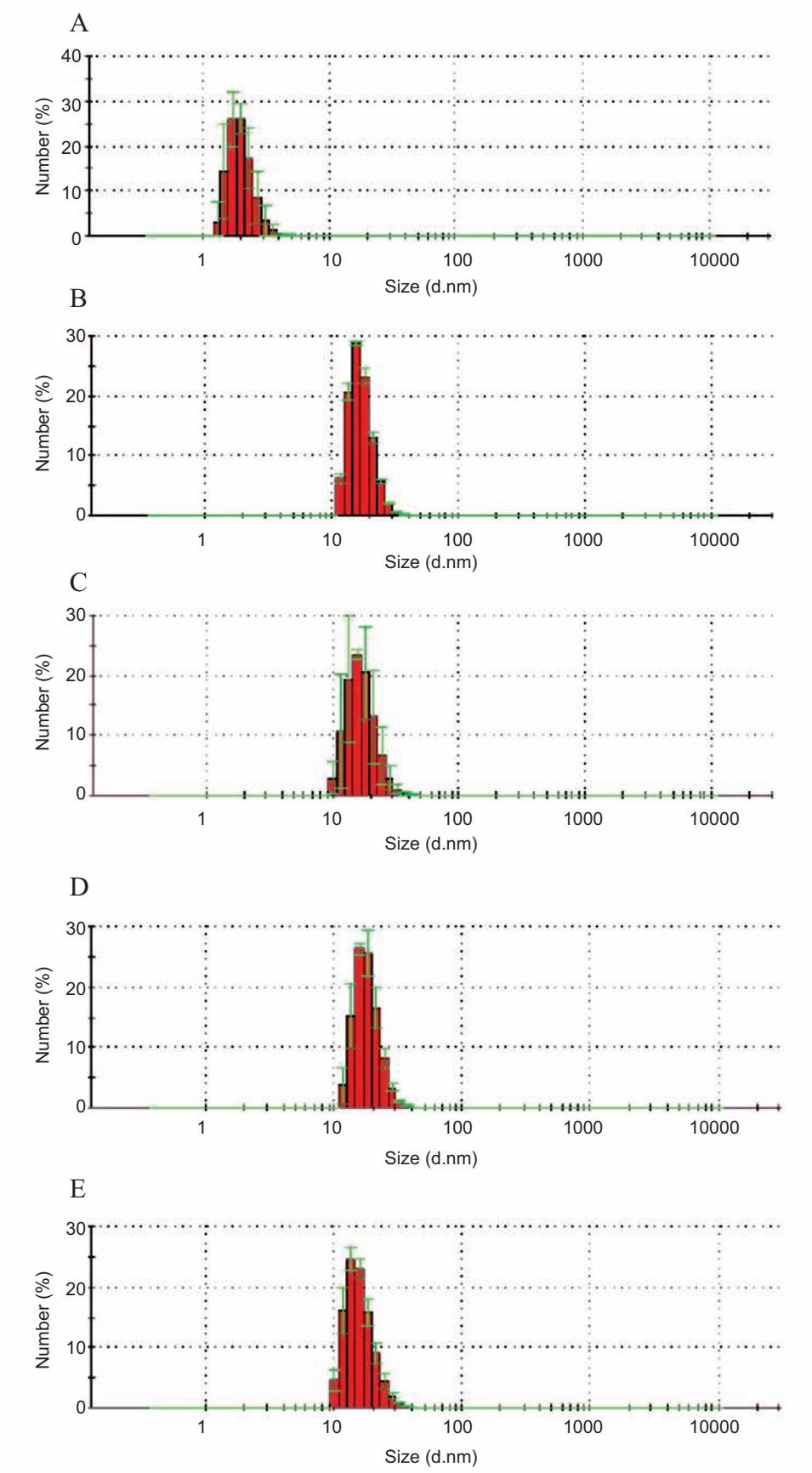

Fig. (2). The sizes of CPP/QD complexes measured by a Zetasizer. The sizes of QDs alone (**A**), SR9/QD (**B**), HR9/QD (**C**), PR9/QD (**D**), and IR9/QD (**E**) complexes were shown. The molecular ratio of these complexes was 60.

30 min to 5 h (Fig. **8D**). The increase of colocalization between PR9/QD complexes and lysosomes was time-dependent. These data reveal that PR9/QD complexes are trapped in lysosomes, while HR9/QD complexes are not.

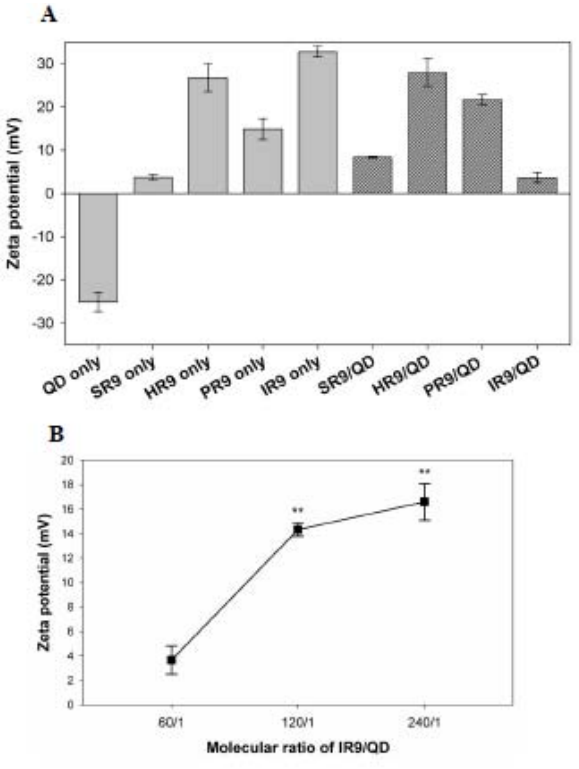

Fig. (3). Zeta-potentials of different CPP/QD complexes. (**A**). Zeta-potentials of QDs, CPPs, and CPP/QD complexes. Various CPPs complexed with QDs prepared at a molecular ratio of 60. (**B**). Comparison of zeta-potentials of IR9/QD complexes prepared at various molecular ratios. IR9 and QDs were combined at molecular ratios of 60, 120, and 240. The value of complexes prepared at a ratio of 60 was served as the control, and each value of zeta-potential in complexes prepared at ratios of 120 and 240 was compared with the control. Significant differences at $P < 0.01$ (**) are indicated. Data are presented as mean ± SD from three independent experiments in each group.

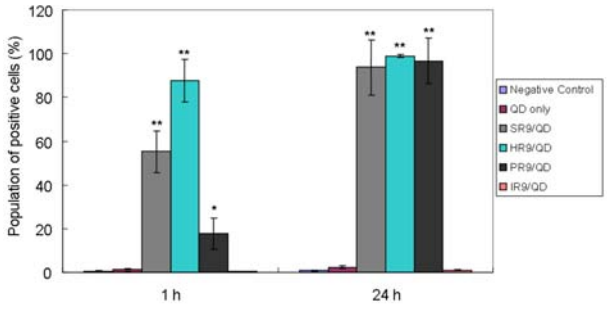

Fig. (4). CPP-mediated QDs delivery into A549 cells. Cells were treated with QDs alone, SR9/QD, HR9/QD, PR9/QD, or IR9/QD complexes for 1 and 24 h. The molecular ratio between CPPs and QDs was 60/1. The fluorescent intensity was analyzed using a flow cytometer. Data are presented as mean ± SD from seven independent experiments in each treatment group.

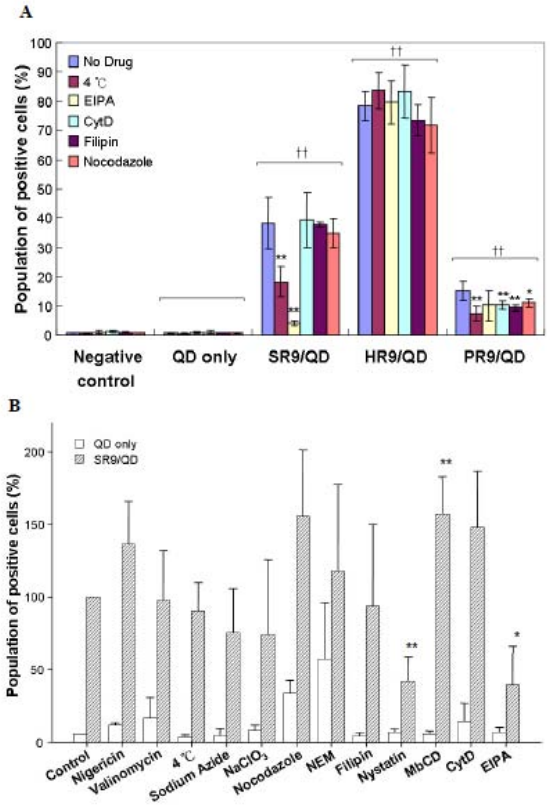

Fig. (5). Mechanisms of the cellular internalization of CPP/QD complexes. (**A**). Penetration efficiency of CPP/QD complexes treated by different endocytosis inhibitors. A549 cells were treated with mock, QDs alone, SR9/QD, HR9/QD, or PR9/QD complexes in the absence or presence of physical or chemical endocytosis inhibitors, respectively. Cells were analyzed using a flow cytometer after a 30 min treatment. (**B**). Detailed analysis of mechanisms in cellular uptake of SR9/QD complexes. Cells were treated with various agents (nigericin, valinomycin, 4℃, sodium azide, sodium chlorate, nocodazole, NEM, filipin, nystatin, MβCD, CytD, and EIPA) for 1 h, respectively. Each group was compared to the control, and each group in QDs or CPP/QD complexes was compared with the group with no drug treatment. Significant differences at $P < 0.05$ (*, †) and $P < 0.01$ (**, ††) are indicated. Data are presented as mean ± SD from seven independent experiments in each treatment group.

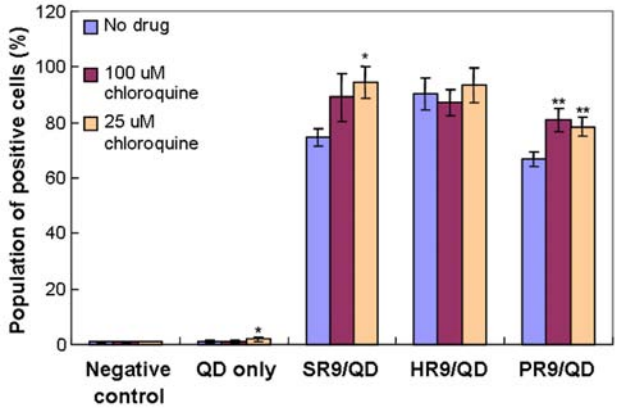

Fig. (6). Effect of a lysosomotropic agent in the delivery of CPP/QD complexes. Cells were treated with QDs alone, SR9/QD,

HR9/QD, or PR9/QD complexes in the absence or presence of chloroquine (25 μM or 100 μM) for 2 h. Cells without any QDs or CPPs treatment were served as the negative control. Each agent-treated group was compared with the group without any drug treatment. Population of positive cells (*y-axis*) in different complexes (*x-axis*) is represented by mean ± SD from three independent experiments in each treatment group. Significant differences at $P < 0.05$ (*) and $P < 0.01$ (**) are indicated.

Our results strongly indicate that the mechanism of HR9-mediated QDs transduction is direct membrane translocation, while PR9-mediated QDs transduction is endocytosis. To further support our findings, immunofluorescent staining of early endosome was utilized. Few yellow dots were found at a 30 min treatment of PR9/QD complexes, while large amounts of clearly yellow dots displayed at a 4 h treatment of PR9/QD complexes (Fig. **9**). The number of dots suggested that colocalization of PR9/QD complexes with endosomes reached the largest at a 4 h incubation, but complexes seemed to disassociate with endosomes at 5 h (Fig. **9**).

Cytotoxicity of CPP/QD Complexes

To assess cytotoxicity by the SRB assay, cells were treated for 24 h with CPP/QD complexes. CPP/QD complexes (CPPs including SR9, HR9, and PR9) prepared at a molecular ratio of 60 did not reduce cell viability (Fig. **10**).

DISCUSSION

In this study, we first demonstrated that CPPs are able to interact with QD nanoparticles and form stably noncovalent complexes *in vitro*. We investigated mechanisms of cellular

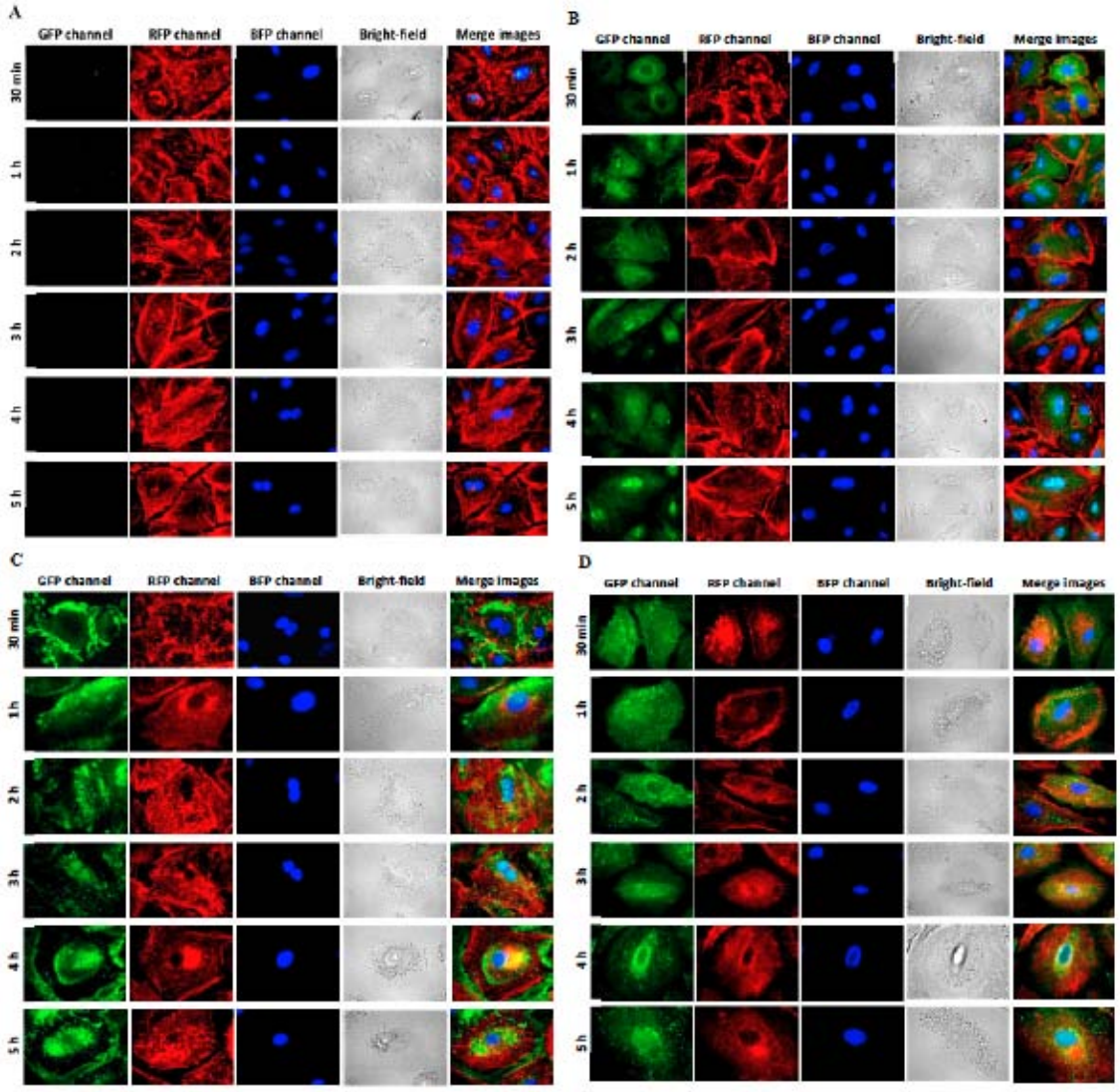

Fig. (7). Colocalization of CPP/QD complexes with F-actins. A549 cells were treated with QDs alone (A), SR9/QD (B), HR9/QD (C), and PR9/QD complexes (D) for various periods of time. Cells were harvested at 30 min, 1, 2, 3, 4, and 5 h, and stained with Texas Red-X Phalloidin and Hoechst. GFP, RFP and BFP channels revealed the distribution of QDs, F-actins and nuclei, respectively. Overlaps between QDs and organelle trackers exhibit yellow color in merged GFP and RFP images, while overlaps between QDs and nuclei show cyan color in merged GFP and BFP images. Cell morphologies were shown in bright-field images. Images were taken using a BD pathway system at a magnification of 600×.

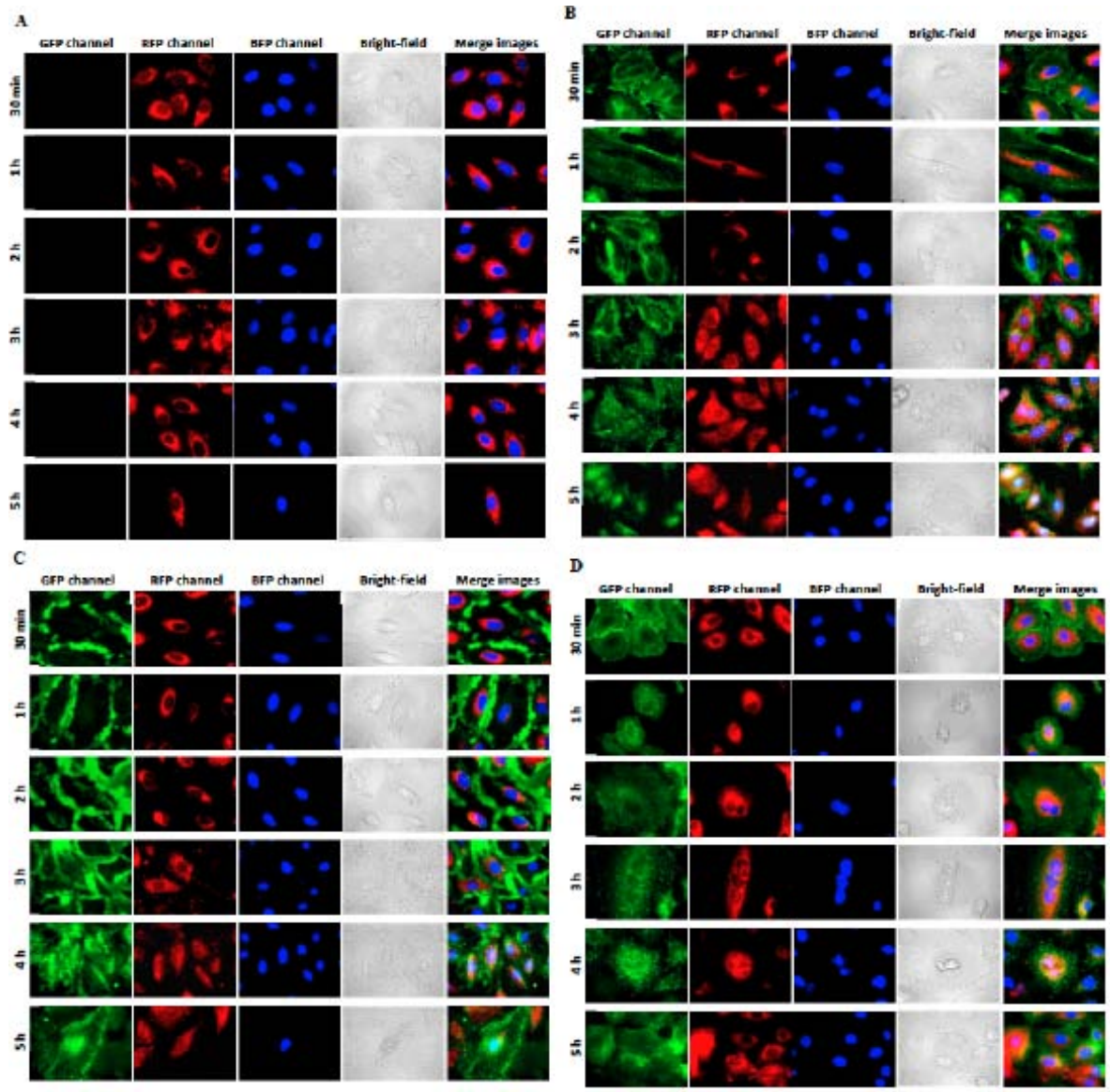

Fig. (8). Colocalization of CPP/QD complexes with lysosomes. A549 cells were treated with QDs alone (**A**), SR9/QD (**B**), HR9/QD (**C**), and PR9/QD complexes (**D**) for various time. Cells were harvested at 30 min, 1, 2, 3, 4, and 5 h, and stained with LysoTracker and Hoechst. GFP, RFP and BFP channels revealed the distribution of QDs, lysosomes and nuclei, respectively. Overlaps between QDs and organelle trackers exhibit yellow color in merged GFP and RFP images, while overlaps between QDs and nuclei show cyan color in merged GFP and BFP images. Cell morphologies were shown in bright-field images. Images were taken using a BD pathway system at a magnification of 600×.

internalization, subcellular localization, and cytotoxicity of these CPP/QD complexes. Pathways of cellular internalization influence delivery efficiency. We found 1) SR9/QD complexes entered cells via a combination of multiple pathways, 2) PR9/QD complexes translocated into cells by energy-dependent classical endocytosis, and 3) HR9/QD complexes utilized energy-independent direct membrane translocation [40, 44]. According to our current results and previous studies, compositions of CPPs are a major factor affecting uptake routes and efficiency, while types of cargoes, manners for complex formation, and surface charges are minor factors [56]. It has been shown that numbers of positive charges, conformations, lengths, hydrophobicities, and concentrations of CPPs influence cellular entry [57]. Properties of cargoes and types of chemical linkage with CPPs are also factors for cellular translocation [57, 58]. Other factors, such as cell types, temperature, and incubation time, also determine major routes of cell-uptake [57, 58].

Endocytosis and direct membrane translocation are two major routes of cellular uptake. Takeuchi *et al.* demonstrated that molecules penetrating cells with direct membrane translocation can pass through membranes within a few minutes at both 4℃ and 37℃ [59].

Cytosolic distribution of CPP/cargo complexes, without endosomal colocalization, was achieved within 1-3 min. As it requires 5-15 min to form endosomes, Goda *et al.* concluded that phospholipid polymers utilized direct membrane translocation to enter HepG2 cells in five min [60]. Therefore, setting a time point at 4 min as the determinant for direct translocation should be reasonable. Our results indicated direct membrane translocation for HR9/QD com-

plexes because of their initial high rate of entry, relative efficiency of translocation and insensitivity to endocytic modulators and lysosomotropic agents [40].

Endocytosis is classified into phagocytosis and pinocytosis. The former involves uptake of large particles, while the latter is the way to internalize solute [57]. Pinocytosis includes macropinocytosis, clathrin-dependent, caveolin-dependent, and clathrin/caveolin-independent pathways [61]. Pharmacological and physical inhibitors are common tools used to distinguish these mechanisms. Cellular entry of PR9/QD complexes was affected by all endocytic inhibitors, except EIPA, indicating the mechanism of classical endocytosis. The cellular uptake mechanism of SR9/QD complexes was more complex. Cellular entry of SR9/QD complexes was inhibited by EIPA and 4℃, suggesting that the mechanism shall be macropinocytosis. However, CytD did not affect macropinocytosis [62]. Further, penetration of SR9/QD complexes for longer time was only affected by nystatin, MβCD, and EIPA. Our data suggested that SR9/QD complexes might enter cells by multiple internalization pathways with the following order: macropinocytosis > caveolae-dependent endocytosis > clathrin-dependent endocytosis [63]. How cells use various pathways in a dynamic manner remains to be elucidated.

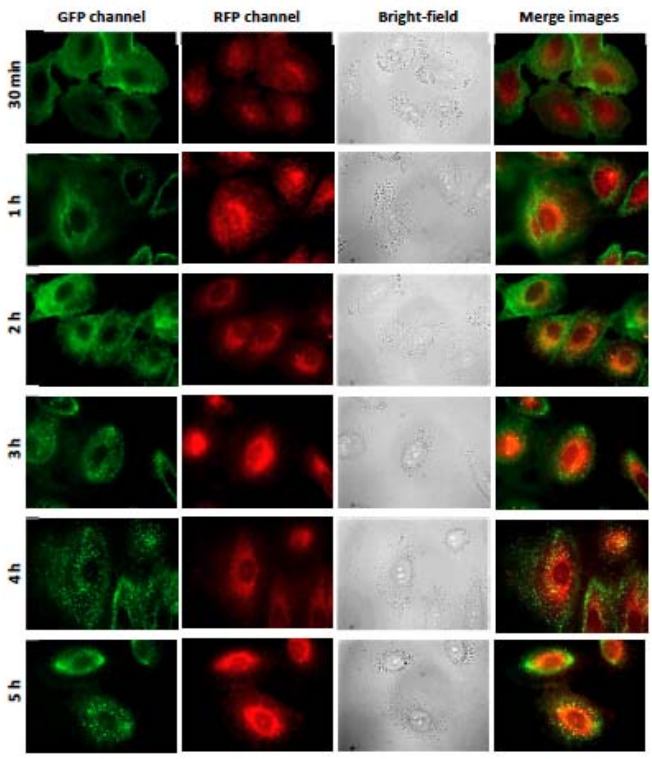

Fig. (9). Colocalization of PR9/QD complexes with early endosome antigen 1 (EEA1) protein. A549 cells were treated with PR9/QD complexes for various time. Immunofluorescent staining of EEA1 was then used. GFP and RFP channels revealed the distribution of QDs and EEA1, respectively.

Chloroquine enhanced the release of SR9/QD and PR9/QD complexes from macropinosomes or endosomes. There are four types of endosomal escape: pore formation, proton sponge effect, fusion with endosomal membrane, and photochemical disruption [64]. Chloroquine and histidine-rich Tat peptides were protonation molecules that busted endosomal membranes [65, 66]. The escape mechanism of PR9/QD complexes should involve both proton spongy effect and membrane fusion. Further, upon being protonated, arginine-rich CPP peptides contain poly-amine groups that act as a detergent in endosomes, leading disruption of endosomal membrane for more efficient delivery [65].

This study provides insights into the mechanisms of CPP-mediated cargo delivery and cellular trafficking of delivered cargoes. HR9-mediated QD delivery was the fastest, most efficient, resulting from its mechanism of direct membrane translocation. Although SR9- and PR9-mediated QD delivery would be trapped in subcellular organelles, they could be free from endosomes. No cytotoxicity was observed, thereby SR9, HR9, and PR9 peptides may be a good tool for delivery of drugs and diagnostic molecules.

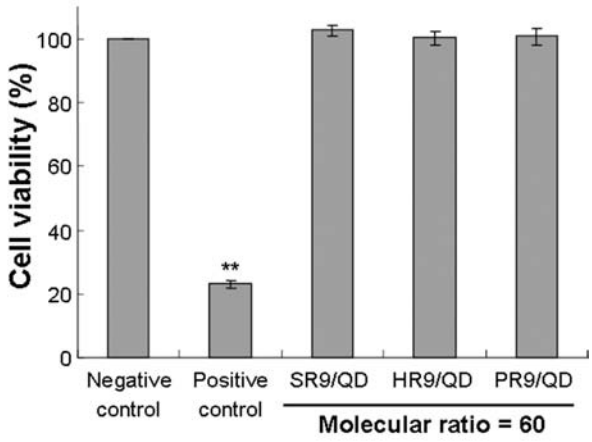

Fig. (10). Cytotoxicity of various compounds and materials. SR9/QD, HR9/QD, or PR9/QD complexes prepared at a molecular ratio of 60 were added into A549 cells for 24 h, respectively. The SRB assay was used for cytotoxic analysis.

CONFLICT OF INTEREST

The authors confirm that this article content has no conflicts of interest.

ACKNOWLEDGEMENTS

We thank Chia-Liang Cheng (Department of Physics, National Dong Hwa University, Taiwan) for performing particle size and zeta-potential measurements and Ryan Morse (Department of Biological Sciences, Missouri University of Science and Technology, Rolla, USA) for technical editing. This work was supported by the Postdoctoral Fellowship NSC 101-2811-B-259-001 (to B.R. L.) and the Grant Number NSC 101-2320-B-259-002-MY3 from the National Science Council of Taiwan (to H.-J. L.).

PATIENT CONSENT

Declared none.

HUMAN/ANIMAL RIGHTS

Declared none.

ABBREVIATIONS

BFP = Blue fluorescent protein

CytD = Cytochalasin D

CPP = Cell-penetrating peptide

EEA1 = Early endosome antigen 1 protein

EIPA = 5-(*N*-ethyl-*N*-isopropyl)-amiloride

GFP = Green fluorescent protein

MβCD = Methyl-β-cyclodetritrin

$NaClO_3$ = Sodium chlorate

NEM = *N*-ethylmaleimide

PBS = Phosphate buffered saline

QD = Quantum dot

RFP = Red fluorescent protein

SD = Standard deviation

SRB = Sulforhodamine B

REFERENCES

[1] Walkey C, Sykes EA, Chan WC. Application of semiconductor and metal nanostructures in biology and medicine. Hematology Am Soc Hematol Educ Program 2009; 701-7.

[2] Schroeder A, Heller DA, Winslow MM, Dahlman JE, Pratt GW, Langer R, Jacks T, Anderson DG. Treating metastatic cancer with nanotechnology. Nat Rev Cancer 2011; 12: 39-50.

[3] Georganopoulou DG, Chang L, Nam JM, Thaxton CS, Mufson EJ, Klein WL, Mirkin CA. Nanoparticle-based detection in cerebral spinal fluid of a soluble pathogenic biomarker for Alzheimer's disease. Proc Natl Acad Sci USA 2005; 102: 2273-6.

[4] Yu SJ, Kang MW, Chang HC, Chen KM, Yu YC. Bright fluorescent nanodiamonds: no photobleaching and low cytotoxicity. J Am Chem Soc 2005; 127: 17604-5.

[5] Chan WC. Maxwell DJ, Goa X, Bailey RE, Han M, Nie S. Luminescent quantum dots for multiplexed biological detection and imaging. Curr Opin Biotechnol 2002; 13: 40-6.

[6] Chen F, Gerion D. Fluorescent CdSe/ZnS nanocrystal-peptide conjugates for long-term, nontoxic imaging and nucleic targeting in living cells. Nano Lett 2004; 4: 1827-32.

[7] Michalet X, Pinaud FF, Bentolila LA, Tsay JM, Doose S, Li JJ, Sundaresan G, Wu AM, Gambhir SS, Weiss S. Quantum dots for live cells, *in vivo* imaging, and diagnostics. Science 2005; 307: 538-44.

[8] Larson DR, Zipfel WR, William RM, Clark SW, Bruchez MP, Wise FW, Webb WW. Water-soluble quantum dots for multiphoton fluorescence imaging *in vivo*. Science 2003; 300: 1434-6.

[9] Delehanty JB, Mattoussi H, Medintz IL. Delivering quantum dots into cells: strategies, progress and remaining issues. Anal Bioanal Chem 2009; 393: 1091-105.

[10] Al-Jamal, WT, Al-Jamal KT, Bomans PH, Frederik PM, Kostarelos K. Functionalized-quantum-dot-liposome hybrids as multimodal nanoparticles for cancer. Small 2008; 4: 1406-15.

[11] Aldana J, Lavelle N, Wang Y, Peng X. Size-dependent dissociation pH of thiolate ligands from cadmium chalcogenide nanocrystals. J Am Chem Soc 2005; 127: 2496-504.

[12] Medintz IL, Uyeda HT, Goldman ER, Mattoussi H. Quantum dot bioconjugates for imaging, labelling and sensing. Nat Mater 2005; 4: 435-46.

[13] Duan H, Nie S. Cell-penetrating quantum dots based on multivalent and endosome-disrupting surface coatings. J Am Chem Soc 2007; 129: 3333-8.

[14] Susumu K, Uyeda HT, Medintz IL, Pons T, Delehanty JB, Mattoussi H. Enhancing the stability and biological functionalities of quantum dots via compact multifunctional ligands. J Am Chem Soc 2007; 129: 13987-96.

[15] Green M, Loewenstein PM. Autonomous functional domains of chemically synthesized human immunodeficiency virus tat transactivator protein. Cell 1988; 55: 1179-88.

[16] Frankel AD, Pabo CO. Cellular uptake of the tat protein from human immunodeficiency virus. Cell 1988; 55: 1189-93.

[17] Elliott G, O'Hare P. Intercellular trafficking and protein delivery by a herpesvirus structural protein. Cell 1997; 88: 223-33.

[18] Yang S, Coles DJ, Esposito A, Mitchell DJ, Toth I, Minchin RF. Cellular uptake of self-assembled cationic peptide-DNA complexes: multifunctional role of the enhancer chloroquine. J Control Release 2009; 135: 159-65.

[19] van den Berg A, Dowdy SF. Protein transduction domain delivery of therapeutic macromolecules. Curr Opin Biotechnol 2011; 22: 888-93.

[20] Wagstff KM, Jans DA. Protein transduction: cell penetrating peptides and their therapeutic applications. Curr Med Chem 2006; 13: 1371-87.

[21] Chang M, Chou JC, Lee HJ. Cellular internalization of fluorescent proteins via arginine-rich intracellular delivery peptide in plant cells. Plant Cell Physiol 2005; 46: 482-8.

[22] Wang YH, Chen CP, Chan MH, *et al.* Arginine-rich intracellular delivery peptides noncovalently transport protein into living cells. Biochem Biophys Res Commun 2006; 346: 758-67.

[23] Hu JW, Liu BR, Wu CY, Lu SW, Lee HJ. Protein transport in human cells mediated by covalently and noncovalently conjugated arginine-rich intracellular delivery peptides. Peptides 2009; 30: 1669-78.

[24] Lu SW, Hu JW, Liu BR, *et al.* Arginine-rich intracellular delivery peptides synchronously deliver covalently and noncovalently linked proteins into plant cells. J Agric Food Chem 2010; 58: 2288-94.

[25] Liu BR, Huang YW, Chiang HJ, Lee HJ. Cell-penetrating peptide-functionized quantum dots for intracellular delivery. J Nanosci Nanotech 2010; 10: 7897-905.

[26] Wei Y, Jana NR, Tan SJ, Ying JY. Surface coating directed cellular delivery of Tat-functionalized quantum dots. Bioconjug Chem 2009; 20: 1752-8.

[27] Guterstam P, Madani F, Hirose H, *et al.* Elucidating cell-penetrating peptide mechanisms of action for membrane interaction, cellular uptake, and translocation utilizing the hydrophobic counter-anion pyrenebutyrate. Biochim Biophys Acta 2009; 1788: 2509-17.

[28] Hoshino A, Fujioka K, Oku T, Nakamura S, Suga M, Yamaguchi Y, Suzuki K, Yasuhara M, Yamamoto K. Quantum dots targeted to the assigned organelle in living cells. Microbiol Immunol 2004; 48: 985-94.

[29] Wadia JS, Dowdy SF. Protein transduction technology. Curr Opin Biotechnol 2002; 13: 52-6.

[30] Deshayes S, Morris MC, Divita G, Heitz F. Cell-penetrating peptides: tools for intracellular delivery of therapeutics. Cell Mol Life Sci 2005; 62: 1839-49.

[31] Wei Y, Jana NR, Tan SJ, Ying JY. Surface coating directed cellular delivery of TAT-functionalized quantum dots. Bioconjug Chem 2009; 20: 1752-8.

[32] Hou YW, Chan MH, Hsu HR, *et al.* Transdermal delivery of proteins mediated by noncovalently associated arginine-rich intracellular delivery peptides. Exp Dermatol 2007; 16: 999-1006.

[33] Liu BR, Chou JC, Lee HJ. Cell membrane diversity in noncovalent protein transduction. J Membrane Biol 2008; 222: 1-15.

[34] Chen CP, Chou JC, Liu BR, Chang M, Lee HJ. Transfection and expression of plasmid DNA in plant cells by an arginine-rich intracellular delivery peptide without protoplast preparation. FEBS Lett 2007; 581: 1891-7.

[35] Wang YH, Hou YW, Lee HJ. An intracellular delivery method for siRNA by an arginine-rich peptide. J Biochem Biophys Methods 2007; 70: 579-86.

[36] Chang M, Chou JC, Chen CP, Liu BR, Lee HJ. Noncovalent protein transduction in plant cells by macropinocytosis. New Phytol 2007; 174: 46-56.

[37] Li JF, Huang Y, Chen RL, Lee HJ. Induction of apoptosis by gene transfer of human TRAIL mediated by arginine-rich intracellular delivery peptides. Anticancer Res 2010; 30: 2193-202.

[38] Liu BR, Li JF, Lu SW, *et al.* Cellular internalization of quantum dots noncovalently conjugated with arginine-rich cell-penetrating peptides. J Nanosci Nanotech 2010; 10: 6534-43.

[39] Xu Y, Liu BR, Lee HJ, *et al*. Nona-arginine facilitates delivery of quantum dots into cells via multiple pathways. J Biomed Biotech 2010; 2010: 948543.

[40] Liu BR, Huang YW, Winiarz JG, Chiang HJ, Lee HJ. Intracellular delivery of quantum dots mediated by a histidine- and arginine-rich HR9 cell-penetrating peptide through the direct membrane translocation mechanism. Biomaterials 2011; 32: 3520-37.

[41] Lee CY, Li JF, Liou JS, Charng YC, Huang YW, Lee HJ. A gene delivery system for human cells mediated by both a cell-penetrating peptide and a piggyBac transposase. Biomaterials 2011; 32: 6264-76.

[42] Dai YH, Liu BR, Chiang HJ, Lee HJ. Gene transport and expression by arginine-rich cell-penetrating peptides in *Paramecium*. Gene 2011; 489: 89-97.

[43] Chen YJ, Liu BR, Dai YH, Lee CY, Chan MH, Chen HH, Chiang HJ, Lee HJ. A gene delivery system for insect cells mediated by arginine-rich cell-penetrating peptides. Gene 2012; 493: 201-10.

[44] Liu BR, Lin MD, Chiang HJ, Lee HJ. Arginine-rich cell-penetrating peptides deliver gene into living human cells. Gene 2012; 505: 37-45.

[45] Liou JS, Liu BR, Martin AL, Huang YW, Chiang HJ, Lee HJ. Protein transduction in human cells is enhanced by cell-penetrating peptides fused with an endosomolytic HA2 sequence. Peptides 2012; 37: 273-84.

[46] Liu MJ, Chou JC, Lee HJ. A gene delivery method mediated by three arginine-rich cell-penetrating peptides in plant cells. Adv Stud Biol 2013; 5: 71-88.

[47] Ziegler A, Nervi P, Durrenberger M, Seelig J. The cationic cell-penetrating peptide CPP (TAT) derived from the HIV-1 protein TAT is rapidly transported into living fibroblasts: optical, biophysical, and metabolic evidence. Biochemistry 2005; 44: 138-148.

[48] Tunnemann G, Ter-Avetisyan G, Martin RM, Stockl M, Herrmann A, Cardoso MC. Live-cell analysis of cell penetration ability and toxicity of oligo-arginines. J Pept Sci 2008; 14: 469-76.

[49] Jones AT. Macropinocytosis: searching for an endocytic identity and role in the uptake of cell penetrating peptides. J Cell Mol Med 2007; 11: 670-84.

[50] Nicola AV, McEvoy AM, Straus SE. Roles for endocytosis and low pH in herpes simplex virus entry into HeLa and Chinese hamster ovary cells. J Virol 2003; 77: 5324-32.

[51] Willingham MC, Pastan I. Endocytosis and exocytosis: current concepts of vesicle traffic in animal cells. Int Rev Cytol 1984; 92: 51-92.

[52] Bharali DJ, Lucey DW, Jayakumar H, Pudavar HE, Prasad PN. Folate-receptor-mediated delivery of InP quantum dots for bioimaging using confocal and two-photon microscopy. J Am Chem Soc 2005; 127: 11364-71.

[53] Caron NJ, Quenneville SP, Tremblay JP. Endosome disruption enhances the functional nuclear delivery of Tat-fusion proteins. Biochem Biophys Res Commun 2004; 319: 12-20.

[54] Michiue H, Tomizawa K, Wei FY, Matsushita M, Lu YF, Ichikawa T, Tamiya T, Date I, Matsui H. The NH2 terminus of influenza virus hemagglutinin-2 subunit peptides enhances the antitumor potency of polyarginine-mediated p53 protein transduction. J Biol Chem 2005; 280: 8285-9.

[55] Moore NM, Sheppard CL, Sakiyama-Elbert SE. Characterization of a multifunctional PEG-based gene delivery system containing nuclear localization signals and endosomal escape peptides. Acta Biomater 2009; 5: 854-64.

[56] Liu BR, Huang YW, Chiang HJ, Lee HJ. Primary effectors in the mechanisms of transmembrane delivery of arginine-rich cell-penetrating peptides. Adv Stud Biol 2013; 5: 11-25.

[57] Madani F, Lindberg S, Langel U, Futaki S, Gräslund A. Mechanisms of cellular uptake of cell-penetrating peptides. J Biophys 2011; 2011: 414729.

[58] Hirose H, Takeuchi T, Osakada H, Pujals S, Katayama S, Nakase I, Kobayashi S, Haraguchi T, Futaki S. Transient focal membrane deformation induced by arginine-rich peptides leads to their direct penetration into cells. Mol Ther 2012; 20: 984-93.

[59] Takeuchi T, Kosuge M, Tadokoro A, Sugiura Y, Nishi M, Kawata M, Sakai N, Matile S, Futaki S. Direct and rapid cytosolic delivery using cell-penetrating peptides mediated by pyrenebutyrate. ACS Chem Biol 2006; 1: 299-303.

[60] Goda T, Goto Y, Ishihara K. Cell-penetrating macromolecules: direct penetration of amphipathic phospholipid polymers across plasma membrane of living cells. Biomaterials 2010; 31: 2380-7.

[61] Conner SD, Schmid SL. Regulated portals of entry into the cell. Nature 2003; 422: 37-44.

[62] Nakase I, Niwa M, Takeuchi T, Sonomura K, Kawabata N, Koike Y, Takehashi M, Tanaka S, Ueda K, Simpson JC, Jones AT, Sugiura Y, Futaki S. Cellular uptake of arginine-rich peptides: roles for macropinocytosis and actin rearrangement. Mol Ther 2004; 10: 1011-22.

[63] Nakase I, Takeuchi T, Tanaka G, Futaki S. Methodological and cellular aspects that govern the internalization mechanisms of arginine-rich cell-penetrating peptides. Adv Drug Deliv Rev 2008; 60: 598-607.

[64] Mandal M, Lee KD. Listeriolysin O-liposome-mediated cytosolic delivery of macromolecule antigen *in vivo*: enhancement of antigen-specific cytotoxic T lymphocyte frequency, activity, and tumor protection. Biochim Biophys Acta 2002; 1563: 7-17.

[65] Miller DK, Griffiths E, Lenard J, Firestone RA. Cell killing by lysosomotropic detergents. J Cell Biol 1983; 97: 1841-51.

[66] Lo SL, Wang S. An endosomolytic Tat peptide produced by incorporation of histidine and cysteine residues as a nonviral vector for DNA transfection. Biomaterials 2008; 29: 2408-14.

Received: January 01, 2013 Revised: January 31, 2013 Accepted: February 07, 2013